SMC5/6-Mediated Plasmid Silencing is Directed by SIMC1-SLF2 and Antagonized by LT

Martina Oravcová[1], Minghua Nie[1], Takanori Otomo[2,3], and Michael N. Boddy[1,3]

[1]Department of Molecular and Cellular Biology, The Scripps Research Institute, La Jolla, CA 92037, USA.

[2]San Diego Biomedical Research Institute, San Diego, CA 92121, USA.

[3]Co-corresponding Authors: nboddy@scripps.edu and totomo@sdbri.org

Running Head: SIMC1 antagonizes plasmid gene expression.

Keywords: SIMC1, C5orf25, Nse5, SLF2, NSMCE5, SMC5, SMC6.

Abstract

SMC5/6 is unique amongst the Structural Maintenance of Chromosomes (SMC) complexes in its ability to repress transcription from extrachromosomal circular DNA (ecDNA), including viral genomes and plasmids. Previously, we showed that human SMC5/6 is regulated by two mutually exclusive subcomplexes—SIMC1-SLF2 and SLF1/2—the counterparts of yeast Nse5/6 (Oravcová, eLife, 2022). Notably, only SIMC1-SLF2 recruits SMC5/6 to SV40 Large T antigen (LT) foci in PML nuclear bodies (PML NBs), suggesting that these regulatory subcomplexes direct distinct roles of SMC5/6 on chromosomal versus ecDNA. However, their roles in plasmid repression remain unclear. Here, we demonstrate that SMC5/6-mediated repression of plasmid transcription depends exclusively on SIMC1-SLF2, whereas SLF1/2 is dispensable. Reinforcing its specialized role in ecDNA suppression, SIMC1-SLF2 does not participate in SMC5/6 recruitment to chromosomal DNA lesions. We further show that plasmid silencing requires a conserved interaction between SIMC1-SLF2 and SMC6, mirroring the functional relationship observed between yeast Nse5/6 and Smc6. As for viral silencing, plasmid repression depends on the SUMO pathway; however, unlike viral silencing, it does not require PML NBs. Additionally, we find that LT interacts with SMC5/6 and increases plasmid transcription to levels observed in SIMC1-SLF2-deficient cells–echoing the antagonistic roles of HBx (HBV) and Vpr (HIV-1) in viral genome repression. These findings expand the paradigm of viral antagonism against SMC5/6-mediated silencing, positioning LT as a novel player in this evolutionary tug-of-war.

Introduction

The Structural Maintenance of Chromosomes (SMC) complexes, present in both prokaryotes and eukaryotes, are core modulators of chromosome architecture and organization, supporting the development and homeostasis of all living organisms (1,2). The SMC1/3 (cohesin) and SMC2/4 (condensin) complexes ensure accurate genome propagation by folding chromosomes into distinct structures. Meanwhile, SMC5/6 plays a key role in maintaining genome stability and integrity, contributing to processes such as homologous recombination (HR), alternative lengthening of telomeres (ALT), and ribosomal DNA (rDNA) replication (3-7). Recently, SMC5/6 has also been recognized as a viral restriction factor, highlighting its broader role in managing extrachromosomal DNAs (ecDNAs, (8-10)).

Beyond viral restriction, the repression of transcription from simple plasmid DNA has also been added to the activities of the human SMC5/6 “Swiss Army knife” of DNA manipulation (8-12). SMC5/6 selectively represses the transcription of circular but not linear plasmid DNA (12), which is likely related to their topological states. That is, DNA that accumulates superhelical stress during transcription is the preferred binding substrate for SMC5/6, whereas linear DNA that dissipates such tension is not stably bound by the complex (12-15). Once DNA bound, SMC5/6 may further compact and thereby restrict transcriptional activity on the ecDNA.

All SMC complexes share a fundamental structure consisting of a SMC heterodimer connected by a kleisin protein. These complexes form a ring-like structure that traps DNA. The SMC proteins have a bent-arm shape and can open to encircle DNA when their ATPase head domains bind ATP, aiding DNA movement through the ring.

60 Kleisin plays a critical role for connecting and locking the SMC heads together (6,16-22).
61 The SMC5/6 complex is particularly adept at recognizing and compacting special DNA
62 structures, such as HR intermediates and supercoiled DNA (13,15,23,24).

63 The SMC5/6 complex is composed of a highly conserved “core” hexamer: the
64 SMC5/6 heterodimer and non-SMC-elements (NSE) 1-4 (9). A Kleisin (Nse4 in yeast;
65 NSMCE4 in human) and two interacting partners (Nse1 and Nse3 in yeast; NSMCE1 and
66 NSMCE3 in human) form a trimer that joins the SMC5/6 head domains. The SUMO ligase
67 Nse2 (NSMCE2 in human) attaches to the SMC5 arm. The complex’s functional
68 specificity is further defined by non-core subunits, the Nse5/6 heterodimer (9,18,25).

69 Yeast Nse5/6 plays key roles in regulating Smc5/6’s genome stability functions,
70 facilitating its chromatin loading, inhibiting its ATPase activity, and enhancing Nse2
71 SUMO ligase activity (19,26-32). Despite its critical regulatory roles, the identification of
72 a human Nse5/6-like complex lagged, largely due to the lack of cross-species protein
73 sequence conservation. Nevertheless, identified in proteomic approaches, the human
74 SLF1 (SMC5-SMC6 Complex Localization Factor 1)-SLF2 heterodimer (SLF1/2) was
75 shown to fulfill some genome stability roles performed by Nse5/6 in yeast (7). Interestingly,
76 however, with the possible exception of HIV-1 proviral DNA, the repression of viral DNA
77 transcription by SMC5/6 depends on SLF2 but not SLF1 (8,9,11). Therefore, SLF2 either
78 functions as a monomer in viral repression, or there is a cofactor that replaces SLF1 in
79 this role. Towards resolving this issue, we recently discovered SIMC1 as a missing link in
80 SMC5/6 regulation and demonstrated that the SIMC1-SLF2 complex is a human
81 counterpart of yeast Nse5/6 (33).

82 Our structural and mutational analyses revealed that SIMC1 and SLF2 contain
83 Nse5 and Nse6-like domains, respectively, which interact through a conserved interface.
84 SIMC1-SLF2 interacts with and directs SMC5/6 to subnuclear compartments at PML
85 nuclear bodies (PML NBs) induced by the SV40 polyomavirus large T antigen (LT).
86 Further, we showed that SIMC1-SLF2 and SLF1/2 are mutually exclusive subcomplexes
87 of SMC5/6 that likely support the distinct antiviral and DNA repair activities of the
88 holocomplex. Thus, SIMC1-SLF2 and SLF1/2 act as Nse5/6-like regulatory elements that
89 modulate the broad activities of the SMC5/6 complex (33).

90 Despite the foregoing advances, the specific roles of the SLF2-based SIMC1 and
91 SLF1 subcomplexes in SMC5/6 regulation remained unclear. Although we previously
92 proposed distinct functions for SIMC1-SLF2 and SLF1/2 in ecDNA silencing and DNA
93 repair, respectively, these mechanisms had yet to be demonstrated. Additionally,
94 SUMOylation, PML NBs, and SV40 LT were implicated in the regulation of SMC5/6-based
95 ecDNA silencing, but their contributions were not fully understood. Here, we address
96 these gaps directly. In line with our prior model, we show that SIMC1-SLF2, but not
97 SLF1/2, mediates plasmid silencing through a direct and evolutionarily conserved
98 interaction with SMC6. Conversely, SLF1/2 specifically recruits SMC5/6 to DNA lesions.
99 Furthermore, we demonstrate that plasmid silencing is facilitated by the SUMO pathway
100 but, unlike the SMC5/6-mediated silencing of HBV (34), does not require PML NBs. Lastly,
101 we reveal that SV40 LT binds SMC5/6 and antagonizes plasmid silencing, thereby adding
102 polyomaviruses to the growing list of pathogenic viruses that counteract SMC5/6-based
103 transcriptional repression.
104

Results

SIMC1-SLF2 associates with SMC6 through a conserved patch

Our previous structural analysis revealed that the Nse5-like domain of SIMC1 ($SIMC1^{Nse5}$) and the Nse6-like domain of SLF2 ($SLF2^{Nse6}$) both adopt α-solenoid-like structures (33). These domains interact in a head-to-tail orientation, forming an ellipsoid-shaped dimer (**Figure 1A**). This dimerization clusters conserved residues from the N-terminus of $SIMC1^{Nse5}$ and the C-terminus of $SLF2^{Nse6}$ at one edge of the ellipsoid (**Figure 1B**). We previously used a SIMC1 mutant harboring four substitutions in α1 of SIMC1 ($SIMC1^{combo}$, **Figure 1B**) to demonstrate that this conserved patch of SIMC1 is essential for binding to SMC6 and for the localization of the SMC5/6 complex at LT-containing PML NBs (33).

In this study, we extended our analysis to SLF2 by introducing two sets of mutations into the Nse6-like region of SLF2 ($SLF2^{CTD}$; residues 635-1173): **mut 1** (E1121A/K1122A/K1125D/C1126R/E1130K in α16) and **mut 2** (T1138R/K1141E/D1142R/A1145R/G1149E in the subsequent loop and α17). These mutations were designed to disrupt charge interactions, hydrogen bonds, and van der Waals contacts, following the same strategy used with $SIMC1^{combo}$ to disrupt binding (33). Using HEK293 cells co-expressing FLAG-tagged $SLF2^{CTD}$ mutants, GFP-tagged SIMC1 and Myc-tagged SMC6, we performed GFP pull-downs followed by Western blot analysis (**Figure 1C**). Wild-type $SLF2^{CTD}$ interacted with both SIMC1 and SMC6 (Lane 1), whereas both **mut 1** and **mut 2** disrupted SMC6 binding while preserving the interaction with SIMC1 (Lanes 2, 3).

We also examined several control mutants. To confirm the specificity of the SIMC1-SMC6 interaction, we introduced a new SIMC1 control mutant containing four

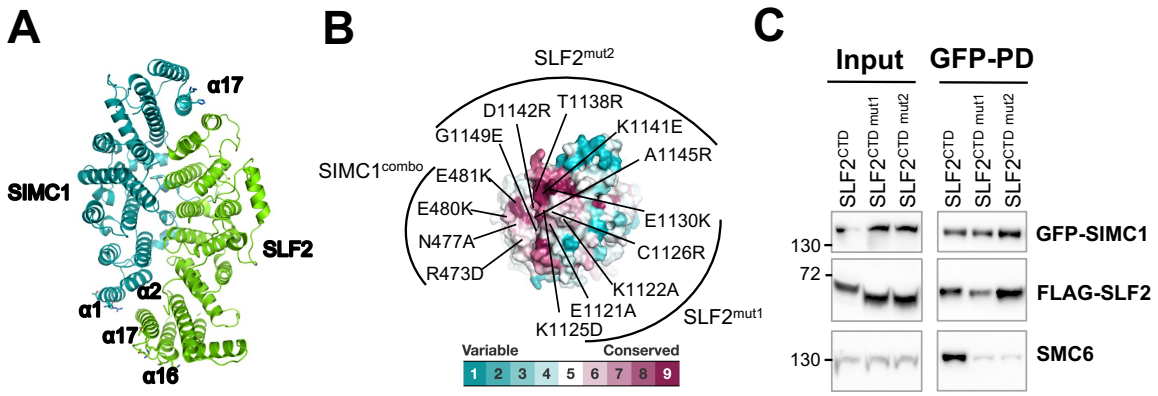

Figure 1: SIMC1-SLF2 composite surface patch is required for SMC6 association. **(A)** The cryo-EM structure of the SIMC1-SLF2 complex (PDB ID: 7T5P) (33). Residues mutated for interaction analysis are shown with side chains. **(B)** Conservation mapping on the surface of SIMC1-SLF2 complex, showing the N-terminus of SIMC1 and the C-terminus of SLF2. Conservation scores obtained from the Consurf server (35) are shown by the color graduation as indicated. Amino acids mutated in SIMC1^{combo} (R473D/N477A/E480K/E481K in α1 of SIMC1), SLF2 mut1 (E1121A/K1122A/K1125D/C1126R/E1130K in α16 of SLF2) and SLF2 mut2 (T1138R/K1141E/D1142R/A1145R/G1149E in α17 of SLF2) are labeled. **(C)** Western blot of GFP-Trap immunoprecipitation from HEK293 cells transfected with plasmids expressing GFP-SIMC1, Myc-SMC6, and FLAG-tagged C-terminal domain (CTD) of SLF2, either WT or containing mutations (mut1, mut2). Input and GFP PD were detected with anti-GFP, FLAG, or SMC6 antibody.

145 substitutions (Q842A/H846A/K849E/D857R) in α17, located at the opposite end of the
146 ellipsoid (**Figure 1A**). This mutant retained binding to both SLF2 and SMC6, indicating
147 that the residues altered in SIMC1^{combo} are specifically required for SMC6 interaction
148 (**Figure 1—figure supplement 1A**). We additionally evaluated the most C-terminal
149 residues of SLF2 (1161–1173), which although conserved, are unstructured; however,
150 deleting these residues (SLF2$^{635-1160}$) did not affect SMC6 binding (**Figure 1—figure**
151 **supplement 1B**). Collectively, these results confirm that the conserved surface patch
152 mediating the SIMC1-SLF2 interaction is essential for binding to SMC6.
153

154 **SIMC1-SLF2 subcomplex contacts the neck region of SMC6**

155 We used AlphaFold-Multimer (36) to predict the structure of the SIMC1-SLF2-SMC6
156 complex (**Figure 2A, Figure 2—figure supplement 1A**). The resulting high-confidence
157 model, as assessed by the predicted aligned error (PAE) plot (**Figure 2—figure**
158 **supplement 1B**), aligns well with mutational data and highlights the conserved surface
159 patch of SIMC1-SLF2 as the interface with SMC6 (**Figure 2A**). SMC6 is a long, hairpin-
160 like polypeptide in which its N- and C-termini fold together to form the ATPase "head"
161 domain at one end. The "hinge" domain at the bending end mediates heterodimerization
162 with SMC5 (**Figure 2—figure supplement 1A**). Connecting the head and hinge is a
163 flexible coiled-coil; the portion adjacent to the head is referred to as the "neck" (**Figure**
164 **2A**).

165 In the model, the conserved SIMC1-SLF2 surface patch interacts with C-terminal
166 residues of SMC6, centered on the neck and opposite the ATPase active site where it
167 dimerizes with SMC5's ATPase domain (21,30). This interface shows excellent shape

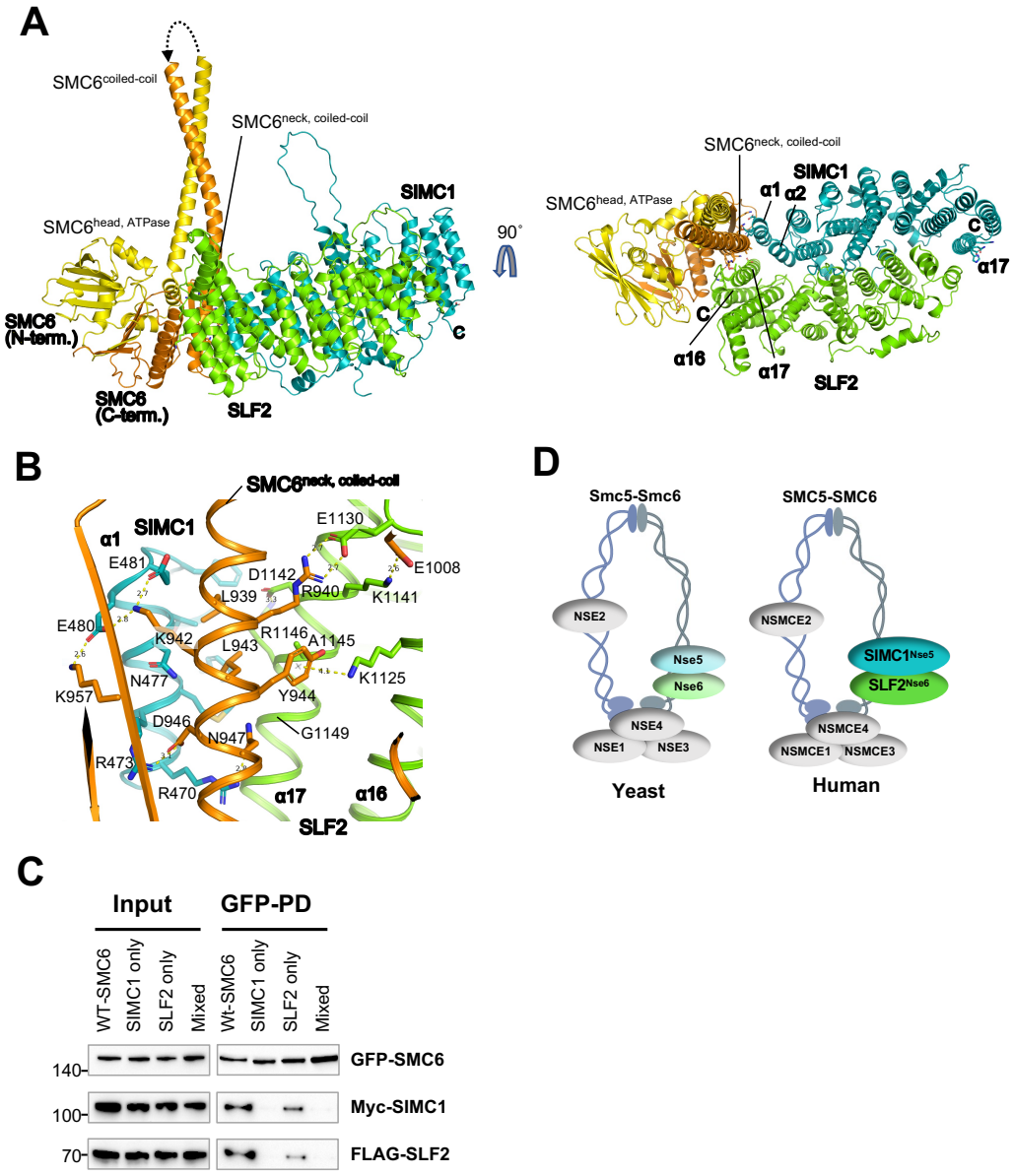

Figure 2: SIMC1-SLF2 subcomplex contacts the neck region of SMC6.
(A) The AlphaFold-Multimer model of the SIMC1^{Nse5}-SLF2^{Nse6}-SMC6 complex. The disordered regions in the N- and C-termini, the hinge domain, and the majority of the coilded-coil that do not contact SIMC1-SLF2 are omitted for clarity. The entire model and the Predicted Aligned Error (PAE) plot of the prediction are shown in **Figure 2 - figure supplement 1**. Residues mutated for interaction analysis are shown with side chains. **(B)** A close-up view of the interface between SMC6's neck and the composite patch of SIMC1-SLF2. **(C)** Western blot of GFP-Trap immunoprecipitation from HEK293 cells transfected with plasmids expressing 2Myc-SIMC1, FLAG-SLF2^{CTD}, and WT or mutant GFP-SMC6 (SIMC1 only: K942A, D946A, K957A; SLF2 only: R940A, Y944A, N947A; Mixed: L939A, R940A, K942A, L943A). Input and GFP PD were detected with anti-GFP, FLAG, or Myc antibody. **(D)** Schematic of yeast (left) and human (right) SMC5/6 complex illustrating positions of its subunits within the complex and Nse5/Nse6 and SIMC1/SLF2 cofactors, respectively, interacting with the neck region of SMC6.

183 complementarity—SMC6's convex neck helix fits snugly into the concave surface formed
184 by α1 and α2 of SIMC1 and α17 of SLF2 (**Figure 2A**). Additional interactions arise from
185 SLF2's α16 and the α16-α17 loop with SMC6's head residues, spanning a total buried
186 surface area of 1516 Å².

187 This model explains the roles of the amino acids altered in our binding studies
188 (**Figure 2B; Figure 2—figure supplement 1C, D**). The four residues modified in
189 SIMC1^{combo} all make direct contact with SMC6's neck helix, including three salt bridges:
190 R473^{SIMC1}-D946^{SMC6}, E480^{SIMC1}-K957^{SMC6}/K942^{SMC6}, and E481^{SIMC1}-K942^{SMC6}. The SLF2
191 mutations also engage SMC6's neck region, forming salt bridges (E1130^{SLF2}-R940^{SMC6}
192 and K1141^{SLF2}-E1008^{SMC6}), a cation-π interaction (K1125^{SLF2}-Y944^{SMC6}), and multiple
193 van der Waals contacts (**Figure 2A; Figure 2—figure supplement 1C, D**). Thus, the
194 model and mutational data are consistent.

195 Next, we validated these SMC6's interface contacts using alanine substitutions.
196 We introduced three sets of mutations: 1) **SIMC1-only** (K942A/D946A/K957A), whose
197 wild-type residues form salt bridges with SIMC1; 2) **SLF2-only** (R940A/Y944A/N947A),
198 where R940 and Y944 interact with SLF2 while N947 forms salt bridges with SIMC1; 3)
199 **Mixed** (L939A/R940A/K942A/L943A), which alters two leucines that insert into a
200 hydrophobic cleft between α1 of SIMC1 and α17 of SLF2, along with two other residues
201 involved in salt bridges (**Figure 2B**). When these SMC6 mutants were co-expressed with
202 SIMC1 and SLF2, pull-down assays showed significantly reduced or abolished binding
203 (**Figure 2C, lane 2-4**). Thus, our mutational data strongly support the AlphaFold model.

204 We conclude that SIMC1-SLF2 associates with the neck region of SMC6, opposite
205 the ATPase active site used for heterodimerization with SMC5 (**Figure 2D; Figure 2—**

206 **figure supplement 1A**). A recent cryo-EM study on the *S. cerevisiae* Smc5/6 complex
207 similarly demonstrated that Nse5/6 engages with the neck region of Smc6 (30),
208 reinforcing the idea that this mode of interaction is evolutionarily conserved (**Figure 2D**).
209 This has implications for the function of SIMC1-SLF2 in the regulation of SMC5/6 activity,
210 based on the findings for yeast Nse5/6 (see discussion).
211
212 **SMC5/6 mediated plasmid silencing requires the Nse5/6-like SIMC1-SLF2 complex**
213 To examine the role of SIMC1 and SLF2 in SMC5/6-mediated episomal DNA silencing,
214 we used CRISPR-Cas9 to create U2OS SIMC1$^{-/-}$ or SLF2$^{-/-}$ cells. We compared the
215 expression of a transfected GFP reporter plasmid between wild-type (WT) and null cells.
216 GFP transcripts, quantified by qPCR, showed a strong increase over WT in both SIMC1$^{-/-}$
217 and SLF2$^{-/-}$ cells (**Figure 3A**). We also used fluorescence activated cell sorting (FACS)
218 to monitor GFP expression (37) and found that both SIMC1$^{-/-}$ and SLF2$^{-/-}$ cells expressed
219 significantly more GFP than WT (**Figure 3B**). In addition to U2OS cells, SIMC1$^{-/-}$ HEK293
220 cells also showed increased GFP reporter expression (**Figure 3—figure supplement 1**).
221 Importantly, expressing WT SIMC1 or SLF2 in the corresponding null cells reduced
222 reporter expression to levels observed in WT cells (**Figure 3B**), demonstrating the
223 involvement of SIMC1-SLF2 in plasmid silencing. Notably, however, SLF2^{mut1} that
224 abolishes SIMC1-SLF2 interaction with SMC6 (**Figure 1C**) did not reduce reporter
225 expression in SLF2$^{-/-}$ cells (**Figure 3B**). These findings demonstrate that SIMC1-SLF2,
226 and their interaction with SMC6, are required for plasmid repression.
227
228
229

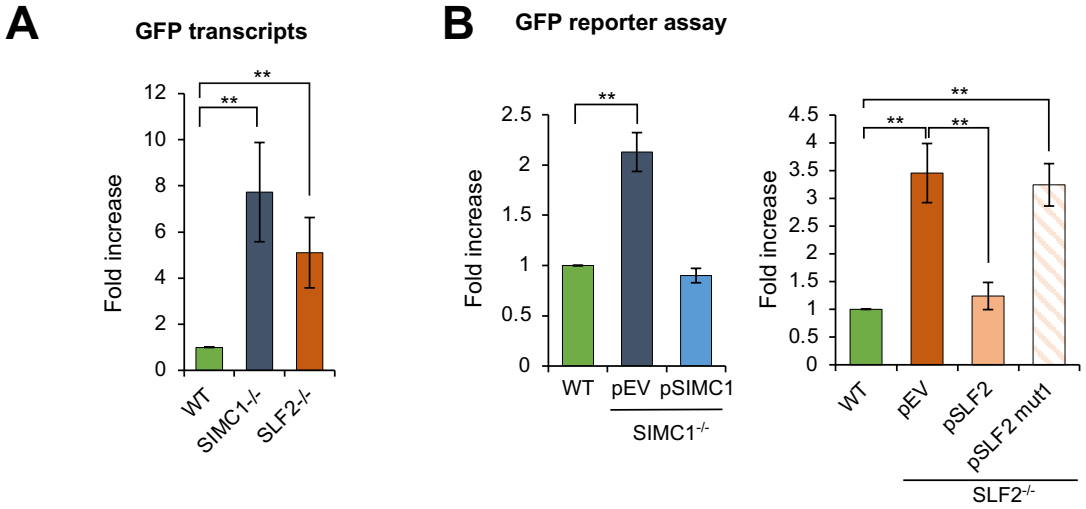

Figure 3: SIMC1/SLF2-SMC6 interaction is critical for plasmid silencing.
(A) Expression of a GFP reporter transiently transfected into U2OS WT and SIMC1$^{-/-}$ or SLF2$^{-/-}$ cell lines was measured by quantitative PCR 72 hours after transfection. GFP expression was normalized to the expression of beta-actin (mean ± s.d. from n=4 independent experiments, two-tailed unpaired t-test; (**) $p<0.005$). **(B)** U2OS WT, SIMC1$^{-/-}$ or SLF2$^{-/-}$ cells with integrated empty vector or vector expressing SIMC1 or SLF2 variants (WT, mut1), respectively, were transiently transfected with GFP reporter. After 72 hours, GFP intensity was measured by FACS and is displayed relative to GFP intensity measured in WT cells. Data are the average ± s.d. from n=3 independent experiments, two-tailed unpaired t-test; (**) $p<0.005$). No significant difference ($p>0.05$) was found between WT and SIMC1$^{-/-}$ + pSIMC1 (left panel), or between WT and SLF2$^{-/-}$ + pSLF2 (right panel).

244 **SIMC1 and SLF1 direct SMC5/6 to plasmid silencing and DNA repair, respectively**

245 We previously showed that SLF1/2 and SIMC1-SLF2 form mutually exclusive complexes
246 with SMC5/6 and recruit it to distinct cellular locations (33). Specifically, epitope-tagged
247 SLF1 colocalized with gamma-H2AX at laser stripes, whereas SIMC1 did not. Here we
248 more directly examined the roles of SLF1 and SIMC1 in recruiting SMC5/6 to DNA
249 damage sites. To this end, we induced localized DNA lesions using laser microirradiation
250 in WT, SLF1$^{-/-}$, and SIMC1$^{-/-}$ U2OS cells. In WT and SIMC1$^{-/-}$ cells SMC5/6 accumulated
251 at laser-induced lesions marked by gamma-H2AX, whereas no such accumulation was
252 seen in SLF1$^{-/-}$ cells (**Figure 4A**). Thus, SLF1 but not SIMC1 plays a critical role in
253 directing SMC5/6 to DNA damage sites. Conversely, when comparing GFP reporter
254 expression in WT and SLF1 null cells, we found no change in GFP levels in the absence
255 of SLF1 (**Figure 4B**). Thus, unlike SIMC1, SLF1 does not play a role in SMC5/6-mediated
256 plasmid silencing, which is consistent with what has been observed in SLF1$^{-/-}$ HepG2
257 cells (10).

258

259

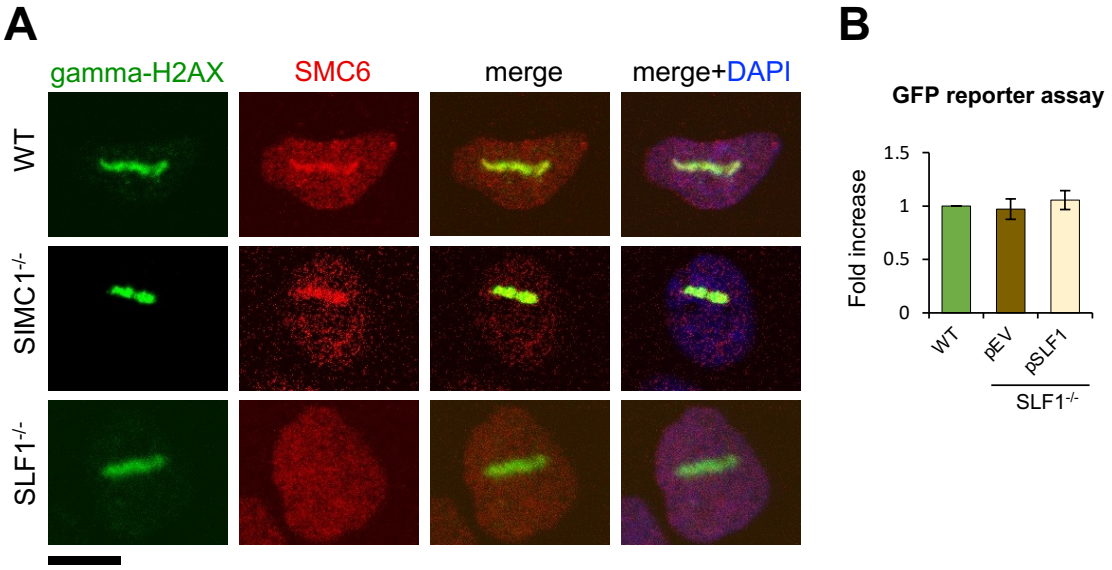

Figure 4: SLF1 is involved in SMC5/6 DNA damage repair, not plasmid silencing. **(A)** Representative immunofluorescence images of U2OS WT, SIMC1$^{-/-}$, SLF1$^{-/-}$ cells exposed to laser microirradiation upon treatment with 50 uM angelicin and 1 ug/ml Hoechst 33342 for 30 min. One hour after microirradiation, cells were pre-extracted, fixed and stained with gamma-H2A.X (phosphorylation of histone H2A.X Ser139; green), SMC6 (red) antibodies and DAPI (blue). Scale bar 10 μm. **(B)** GFP intensity was measured by flow cytometry 72 hr after reporter transient transfection in U2OS WT cells or SLF1$^{-/-}$ cells with integrated empty vector or stably expressing SLF1. Data are the average ± s.d. from n=3 independent experiments, two-tailed unpaired t-test (p-value >0.05).

272 **SUMOylation supports plasmid repression**

273 Given that SIMC1 contains SIMs, and the SMC5/6 complex is a SUMO ligase that
274 contains other SUMO-interacting interfaces, we also tested for a potential involvement of
275 the SUMO pathway in plasmid silencing (33,38,39). Cells were treated with the SUMO
276 pathway inhibitor (SUMOi), TAK981 (40). We observed a strong dose-dependent
277 increase in reporter gene expression in both U2OS and RPE cells (**Figure 5—figure**
278 **supplement 2**), supporting an involvement of the SUMO pathway in plasmid silencing.
279 This is consistent with the broadly observed transcriptionally repressive activity of
280 SUMOylation (41,42). Interestingly, SUMOi treatment does not significantly increase the
281 level of GFP reporter expression in SIMC1$^{-/-}$ and SLF2$^{-/-}$ over its effect on WT, despite the
282 pre-existing defect in plasmid silencing in SIMC1 and SLF2 null cell lines (**Figure 5A**).
283 The lack of additivity between SUMOi and SIMC1$^{-/-}$ or SLF2$^{-/-}$ suggests that SMC5/6-
284 mediated plasmid silencing operates in large part under the broad “umbrella” of
285 SUMOylation-based transcriptional repression.

286

287

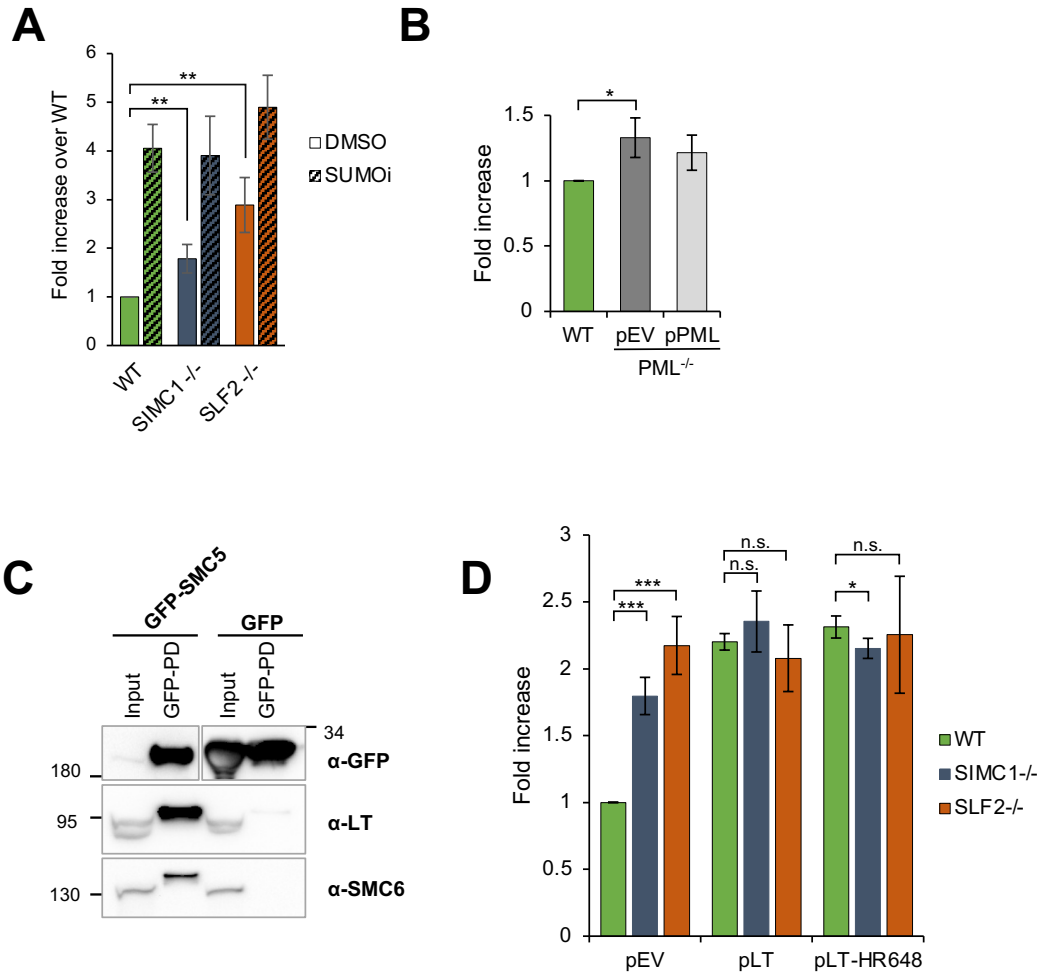

Figure 5: Plasmid silencing depends on the SUMO pathway and LT, not PML NBs. **(A)** U2OS WT, SIMC1$^{-/-}$ or SLF2$^{-/-}$ cells were transiently transfected with GFP reporter and treated with 100 nM TAK-981(SUMOi) or DMSO at the same time. After 72 hours, GFP intensity was determined by FACS. Data are normalized to WT cells treated with DMSO and represent the average ± s.d. from n=4 independent experiments, two-tailed unpaired t-test; (**) p<0.005. No significant difference was found between WT and SIMC1$^{-/-}$ or SLF2$^{-/-}$ when treated with SUMOi (p>0.05). **(B)** U2OS WT or PML$^{-/-}$ cells with integrated empty vector or vector expressing PML, respectively, were transiently transfected with GFP reporter. Intensity of GFP was measured by FACS 72 hours after transfection. Data are the average ± s.d. from n=3 independent experiments, two-tailed unpaired t-test; (*) p<0.05). No significant difference (p>0.05) was found between WT and PML$^{-/-}$ + pPML. **(C)** Western blot of GFP-trap immunoprecipitation from HEK293 cells transiently transfected with either GFP-SMC5 or GFP alone in combination with SV40 vector expressing LT and Myc-SMC6. Signals were visualized using GFP, LT and SMC6 antibodies. **(D)** GFP intensity measured by FACS in U2OS WT, SIMC1$^{-/-}$ or SLF2$^{-/-}$ cells with integrated empty vector, vector expressing large T antigen (LT) or LT-HR684 variant, respectively that were transiently transfected with GFP reporter for 72 hours. Data are the average ± s.d. from n=4 independent experiments. (∗) p<0.05; (∗∗∗) p<0.0005; (n.s.) p>0.05 (two-tailed unpaired t-test).

308 **PML NBs are not required for plasmid silencing**

309 We previously showed that SIMC1-SLF2 directs SMC5/6 to LT antigen-containing SV40
310 replication centers at PML NBs (33). Moreover, SMC5/6-mediated restriction of HBV
311 occurs at PML NBs (34,43) and, the localization of SMC5/6 at PML NBs is SLF2-
312 dependent in HepG2 and PHH cells (10,43). We also now find that SLF2 is required for
313 the localization of SMC5/6 to PML NBs in U2OS cells (**Figure 5—figure supplement 1**).
314 Based on the foregoing, PML NBs have been proposed, but not directly shown, to support
315 simple plasmid repression (10). Therefore, we tested the impact of PML NBs on plasmid
316 silencing by measuring GFP reporter expression in WT and PML$^{-/-}$ U2OS cells (44).
317 Compared to SIMC1 and SLF2 null cells, we observed only a minor increase in GFP
318 expression in PML$^{-/-}$ versus WT cells (**Figure 5B**). Moreover, the stable re-expression of
319 PML in PML$^{-/-}$ cells did not significantly reduce the level of GFP expression, as compared
320 to vector control, suggesting the slight increase observed is due to clonal variation from
321 CRISPR editing (**Figure 5B**). Thus, we conclude that PML NBs are not needed for the
322 SMC5/6-mediated silencing of plasmids.

323

324 **SV40 Large T antigen (LT) overcomes plasmid silencing**

325 Considering that HBx and Vpr antagonize SMC5/6 to induce HBV and HIV-1 transcription,
326 respectively (45-47), we tested if SV40 LT similarly impacts plasmid silencing. In this
327 regard, we previously found that SMC5/6 colocalizes with LT-induced nuclear foci at PML
328 NBs in a SIMC1-SLF2-dependent manner (33). Here, we show that ectopically expressed
329 LT coimmunoprecipitates with GFP-SMC5/6 but not a GFP control (**Figure 5C**). Therefore,
330 LT, like HBx and Vpr, may contact SMC5/6 to antagonize its ecDNA repression activity.

331 Indeed, the stable expression of LT in WT cells promoted GFP reporter plasmid
332 expression, as compared to WT cells with an empty vector control (**Figure 5D; Figure 5–**
333 **figure supplement 3**). The host range defective mutant LT-HR684 had a similar effect
334 as WT LT, indicating that the C-terminus of LT, which inhibits the SV40 host range
335 restriction factor FAM111A (48), is not involved in overcoming plasmid repression (**Figure**
336 **5D**). Notably, the enhancement of plasmid DNA transcription by LT is not additive with
337 that already present in SIMC1$^{-/-}$ and SLF2$^{-/-}$ cells (**Figure 5D**). The epistatic relationship
338 between the positive effects of SIMC1$^{-/-}$, SLF2$^{-/-}$, and LT expression on plasmid
339 transcription indicates that LT overcomes SMC5/6-mediated repression.
340

341 **Discussion**

342 Our structural analyses indicate that SIMC1-SLF2 engages the SMC5/6 core at the neck
343 region of SMC6, situated opposite the ATPase active site. These findings, together with
344 recent cryo-EM analyses of the *S. cerevisiae* Smc5/6 complex (20,21,31), highlight a
345 conserved mode of interaction in which Nse5/6 or Nse5/6-like subunits bind to the
346 backside of SMC6's head domain. This binding site is ideal for allosteric regulation of the
347 ATPase and DNA-binding functions of the SMC5/6 family. Indeed, yeast Nse5/6 reduces
348 Smc5/6 ATPase activity and disrupts the Nse4 (kleisin)-Smc6 interface, which may open
349 the gate to enable topological DNA binding by Smc5/6 (**Figure 6**, (20,30,31)). The clear
350 overlap between our validated SIMC1-SLF2-SMC6 structure and that of yeast Nse5/6-
351 Smc6 suggests that SIMC1-SLF2, and its orthologue SLF1/2, may similarly modulate
352 SMC5/6 ATPase and DNA binding activities, albeit at distinct DNA targets.
353

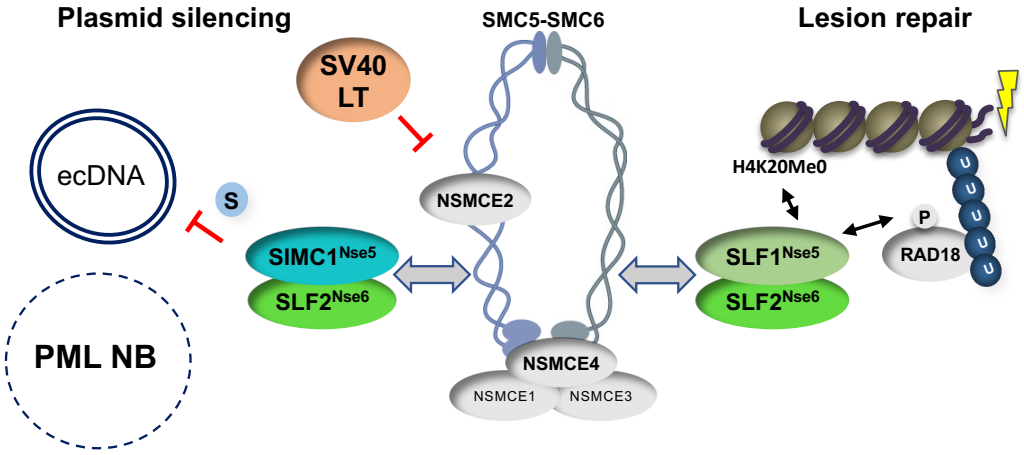

Figure 6: SIMC1-SLF2 and SLF1/2 subcomplexes direct SMC5/6 to separate pathways of plasmid silencing and DNA lesion repair. SIMC1-SLF2 and SMC5/6-mediated plasmid silencing is facilitated by the SUMO pathway and antagonized by SV40 LT. PML NBs are not involved in plasmid silencing. S stands for SUMO; U for ubiquitin. Both SIMC1-SLF2 and SLF1/2 likely contact SMC6 directly through their conserved Nse5/6-like domains, but the SIMC1 SIMs and SLF1 BRCT/ARD domains contact distinct posttranslational modifiers to direct the complex to its separate roles.

363 The distinct targeting functions of the SIMC1 and SLF1-based SLF2 complexes is
364 underscored by our current analysis of microirradiated cells that lack each complex
365 (**Figure 4**). While the deletion of SLF1 abrogates SMC5/6 localization at DNA lesions, the
366 loss of SIMC1 has no effect (**Figure 4A**). On the other hand, SIMC1 is required for the
367 recruitment of SMC5/6 to LT-containing PML NBs (33). Lastly, we found that SLF1 does
368 not impact plasmid silencing (**Figure 4B**), consistent with several analyses of HIV-1, rAAV,
369 and HBV silencing (10,43,45,49) but contrasting with another study (50). It remains
370 unclear why this latter discrepancy exists. While there may still be overlapping functions
371 of SIMC1 and SLF1 to uncover at the organismal level, it is clear they support distinct
372 cellular responses to ecDNAs and DNA lesions (**Figure 6**).
373 In keeping with the SUMO-binding ability of SIMC1 (**Figure 6**, (39)), we found that
374 the inhibition of SUMOylation by TAK-981 strongly enhanced plasmid transcription
375 (**Figure 5–figure supplement 2**). This is likely a broad effect that includes the loss of
376 repressive modifications of transcription factors (42); as well as the lifting of SMC5/6-
377 mediated repression to enhance ecDNA transcription. A similar effect of TAK-981 was
378 seen on HIV-1 proviral DNA gene expression, which was elevated by SUMO inhibition to
379 a similar degree as that observed in SMC5Δ cells (50). The authors concluded that the
380 effect of TAK-981 was entirely through the inhibition of SMC5/6-mediated SUMOylation
381 (NSE2 subunit). This is different to our results, which show that SUMOylation inhibition
382 has a larger effect than the loss of the SIMC1-SLF2 complex on plasmid gene expression.
383 The distinct natures of the ecDNAs under study, plasmid versus HIV-1 proviral DNA, and
384 the genetic backgrounds may contribute to this difference. Nevertheless, our data support
385 a key role of the SUMO pathway in plasmid repression, and that SMC5/6 works within it.

386 Despite the fact that SIMC1-SLF2 localizes SMC5/6 to PML NBs that contain SV40
387 LT (31), and HBV is restricted at PML NBs (34), they are dispensable for plasmid silencing.
388 While the reason for the different impact of PML NBs in HBV versus simple plasmid
389 silencing remain unknown, it may be related to the natural localization of each ecDNA.
390 That is, HBV localizes to PML NBs as part of the viral life cycle, in a manner dependent
391 on the SUMOylation of its core protein (51). In contrast, the direct visualization of plasmids
392 revealed they are pan-nuclear and apparently excluded from PML NBs (52). It is also
393 noteworthy that a recent genome-scale CRISPR screen for repressors of rAAV
394 transcription identified all components of the SMC5/6 complex, including SIMC1 and
395 SLF2, but not SLF1 or PML (49). This raises interesting questions about the mechanism
396 of SMC5/6-mediated transcriptional silencing, since it can occur outside PML NBs. In this
397 regard, SUMOylation was recently shown to support the recombination-based alternative
398 lengthening of telomeres (ALT) pathway in the absence of PML NBs (53), which are
399 normally key components of the fully active pathway (44). Therefore, the SUMOylation of
400 plasmid associated proteins, and or SMC5/6, may support transcriptional repression of
401 plasmids in the absence of PML NBs, consistent with our findings using TAK-981.
402 Interestingly, the expression of LT enhances plasmid transcription in a non-additive
403 manner with the deletion of SIMC1 or SLF2, suggesting an epistatic relationship. While
404 LT is known to be a promiscuous transcriptional activator (54,55) that does not rule out a
405 co-existing role in antagonizing SMC5/6. Indeed, these findings are reminiscent of HBx
406 from HBV and Vpr of HIV-1, both of which are known promiscuous transcriptional
407 activators that also directly antagonize SMC5/6 to relieve transcriptional repression
408 (12,45-47,56-58). Unlike HBx and Vpr, the interaction of LT with SMC5/6 does not appear

409 to induce the degradation of its subunits (33). Nevertheless, LT binds and sterically
410 inhibits several cellular proteins instead of inducing their degradation, including Rb and
411 p53 (59). Further analysis will be needed to define LT-SMC5/6 contacts, and its potential
412 mode of inhibition. This will have important ramifications for the lifecycle of the pathogenic
413 polyomaviruses since their LT proteins share functions with SV40 LT (60).

414 In conclusion, our structure-function analyses delineate a specific function for the
415 SIMC1-SLF2 complex in SMC5/6-mediated plasmid repression. This resolves a
416 discrepancy in the field, wherein SLF2 was thought to act alone in ecDNA repression,
417 since SLF1 is not required. While further studies are needed, SIMC1-SLF2 is most likely
418 responsible for supporting SMC5/6-mediated ecDNA silencing, including that of multiple
419 pathogenic viruses. Although HBV silencing requires PML NBs, we find that plasmid
420 silencing does not. This represents a departure from current dogma, suggesting that the
421 SMC5/6-mediated repression mechanism does not always rely on PML NB-resident
422 factors. In some cases, the SUMOylation of ecDNA-associated proteins may be sufficient
423 to support SMC5/6-based repression. Finally, because the SV40 LT antigen interacts with
424 SMC5/6 and antagonizes its repression of plasmids, the orthologous polyomaviral LT
425 antigens are likely to block SMC5/6-mediated restriction of pathogenic polyomaviruses.
426

427 **Material and Methods**

428 **Construction of recombinant plasmids**

429 Construction of plasmid DNA was described in (33). Mutations in SIMC1 (combo ctrl),
430 SLF2 (mut1, mut2) and SMC6 (mixed, SIMC-only, SLF2-only) were either introduced in
431 primers or a gBlock sequence containing desired mutations was purchased (IDT). All
432 plasmids created in this study have been verified by sequencing service provided by
433 Plasmidsaurus. Plasmid used in this study are listed in Appendix 1. Additional details of
434 plasmid construction are available upon request.

435

436 **Cell culture, transfection, stable line generation**

437 All cell lines and their derivatives (see Appendix 1) were cultured in DMEM (Gibco)
438 supplemented with 10% (v/v) fetal bovine serum (Omega Scientific), 1% (v/v) antibiotic-
439 antimycotic (Gibco) and maintained at 37 °C in humidified air with 5% CO_2.
440 Transient plasmid transfections and generation of stable cell lines was detailed in (33). A
441 complete list of stable mammalian cell lines generated, and reagents used in this study
442 is provided (Appendix 1).

443

444 **Cell line generation by CRISPR/Cas9**

445 SIMC1, SLF1 and SLF2 knockout clones were generated via reverse transfection of
446 CRISPR/Cas9 Ribonucleoprotein. A mixture of three sgRNAs specific for each gene
447 (Synthego; 24 nM) was combined with 6 nM Cas9-NLS (Synthego) in reduced-serum
448 medium OptiMEM and incubated for 10 min followed by a 15 min incubation with TransIT-
449 X2 (Mirus). 6 x 10^4 cells were added and plated into 12-well plates. After 72 hours, cells

450 were diluted and plated to isolate single cell clones that were genotyped to confirm
451 successful editing. sgRNA sequences and diagnostic primers used in this study are listed
452 in Appendix 1.
453
454 **Co-immunoprecipitation and Western blotting**
455 GFP-labeled proteins were immunoprecipitated using the Nano-Trap magnetic agarose
456 (Chromotek) following the manufacturer's instructions. The protocol as well as whole cell
457 lysate preparation for SDS-PAGE and western blot are described in detail in (33).
458 Antibodies used for immunoblotting are listed in Appendix 1.
459
460 **RNA extraction and quantitative PCR**
461 For monitoring GFP expression by qPCR, cells were harvested for RNA isolation 72 hours
462 after GFP vector transient transfection. Total RNA precipitated using RNeasy Plus Mini
463 kit (Quiagen) was treated with DNaseI kit (Invitrogen) before cDNA synthesis by
464 SuperScript III First-Strand Synthesis System for RT-PCR (Invitrogen). SensiFAST SYBR
465 No-ROX kit (Meridian Bioscience) was used for qPCR and gene expression was
466 calculated as $2^{-\Delta Ct}$ using beta-actin as a reference. Oligonucleotides are listed in
467 Appendix 1.
468
469 **Flow cytometry**
470 GFP fluorescence measurements were based on (37). GFP reporter vector was
471 transiently transfected into cells using TransIT-LT1 (Mirus). After 72 hours, cells were
472 washed in PBS, dissociated using 0.25% trypsin and resuspended in DMEM. For SUMOi

473 experiments, cells were treated with 100 nM TAK-981 (Cayman Chemical) or 0.1%
474 DMSO in control plates at the time of GFP vector transfection. Median GFP intensity was
475 measured on Cytoflex S (Beckman Coulter) using the CytExpert software. A minimum of
476 1100 GFP-positive cells were analyzed.
477
478 **DNA damage by laser microirradiation**
479 Protocol adapted from (61). U2OS cells (1.5 x 10^5) were plated in a 35 mm µ-Grid dish
480 (Ibidi) a day before microirradiation. Cells were treated with 50 uM angelicin
481 (ThermoFisher) and 1 µg/ml Hoechst 33342 (Invitrogen) for 30 min before transferring to
482 the stage incubator of LSM880 Airyscan confocal laser scanning microscope (Zeiss).
483 Using the bleaching mode in ZEN software, DNA damage was induced by irradiation of
484 a 5-pixel wide region with a 405 nm diode laser (15% power, 1 iteration, zoom 1,
485 averaging 1, pixel dwell time 0.27 µs = speed 7). One hour after the irradiation, cells were
486 treated with extraction buffer (0.5% Triton X-100, 20 mM Hepes, 50 mM NaCl, 3 mM
487 $MgCl_2$, 300 mM sucrose) for 2 min, washed twice in PBS, fixed in 4% formaldehyde in
488 PBS for 15 min and stained with anti-phospho-Histone H2A.X (Ser139) and anti-SMC6
489 antibodies following the immunofluorescence protocol.
490
491 **Immunofluorescence and microscopy**
492 Immunofluorescence and confocal microscopy were done as described (33).
493 For optimal detection of SMC6, we pre-extracted the chromatin with extraction buffer (0.5%
494 Triton X-100, 20 mM Hepes, 50 mM NaCl, 3 mM $MgCl_2$, 300 mM sucrose) for 2 min on
495 ice. Antibodies used in this study are listed in Appendix 1.

496

497 **Luciferase and MTT assays**

498 U2OS cells were seeded at 4 x 10^3 cells per well of a 96-well plate and transfected with
499 20 ng of luciferase reporter plasmid (expresses secreted Gaussian luciferase under
500 EF1alpha promoter) using TransIT-LT1 (Mirus) by reverse transfection. TAK-981 in
501 indicated concentrations or DMSO were added at the time of transfection and Luciferase
502 activities were measured 3 days later. Ten microliters of culture media were mixed with
503 50 ul Gaussia Luciferase Glow Assay buffer that contains freshly diluted coelenterazine
504 substrate (Pierce™ Gaussia Luciferase Glow Assay Kit). Luminescence was measured
505 after ten minutes on a Tecan Infinite M200 plate reader (Tecan Life Sciences). The
506 number of viable cells were estimated using MTT assay kit (Sigma) following
507 manufacturer's instructions.

508

509 **AlphaFold-Multimer Structural modeling**

510 AlphaFold-Multimer modeling (36) was performed using default settings on the following
511 protein sequences: SIMC1^{Nse5} (425-872), SLF2^{Nse6} (733-1173), and SMC6 (1-1091) .

512

513 **Material Availability**

514 All materials produced during this work are available upon written request, in keeping with
515 the requirements of the journal, funding agencies, and The Scripps Research Institute.

516

517

518 **References**

519 1. Hirano T. At the heart of the chromosome: SMC proteins in action. Nat Rev Mol Cell
520 Biol. 2006;7(5):311-22.
521 2. Nasmyth K, Haering CH. The structure and function of SMC and kleisin complexes.
522 Annu Rev Biochem. 2005;74:595-648.
523 3. Peng XP, Lim S, Li S, Marjavaara L, Chabes A, Zhao X. Acute Smc5/6 depletion
524 reveals its primary role in rDNA replication by restraining recombination at fork pausing sites.
525 PLoS Genet. 2018;14(1):e1007129. PMCID: PMC5779651
526 4. Potts PR, Yu H. The SMC5/6 complex maintains telomere length in ALT cancer cells
527 through SUMOylation of telomere-binding proteins. Nat Struct Mol Biol. 2007;14(7):581-90.
528 5. Wehrkamp-Richter S, Hyppa RW, Prudden J, Smith GR, Boddy MN. Meiotic DNA joint
529 molecule resolution depends on Nse5-Nse6 of the Smc5-Smc6 holocomplex. Nucleic Acids
530 Res. 2012;40(19):9633-46. PMCID: PMC3479181
531 6. Aragon L. The Smc5/6 Complex: New and Old Functions of the Enigmatic Long-
532 Distance Relative. Annu Rev Genet. 2018;52:89-107.
533 7. Raschle M, Smeenk G, Hansen RK, Temu T, Oka Y, Hein MY, Nagaraj N, Long DT,
534 Walter JC, Hofmann K, Storchova Z, Cox J, Bekker-Jensen S, Mailand N, Mann M. DNA repair.
535 Proteomics reveals dynamic assembly of repair complexes during bypass of DNA cross-links.
536 Science. 2015;348(6234):1253671.
537 8. Irwan ID, Cullen BR. The SMC5/6 complex: An emerging antiviral restriction factor that
538 can silence episomal DNA. PLoS Pathog. 2023;19(3):e1011180. PMCID: PMC9980727
539 9. Peng XP, Zhao X. The multi-functional Smc5/6 complex in genome protection and
540 disease. Nat Struct Mol Biol. 2023;30(6):724-34. PMCID: PMC10372777

541 10. Abdul F, Diman A, Baechler B, Ramakrishnan D, Kornyeyev D, Beran RK, Fletcher SP,
542 Strubin M. Smc5/6 silences episomal transcription by a three-step function. Nat Struct Mol Biol.
543 2022;29(9):922-31.
544 11. Liu HW, Roisne-Hamelin F, Gruber S. SMC-based immunity against extrachromosomal
545 DNA elements. Biochem Soc Trans. 2023;51(4):1571-83. PMCID: PMC10586767
546 12. Diman A, Panis G, Castrogiovanni C, Prados J, Baechler B, Strubin M. Human Smc5/6
547 recognises transcription-generated positive DNA supercoils. Nat Commun. 2024;15(1):7805.
548 PMCID: PMC11379904
549 13. Serrano D, Cordero G, Kawamura R, Sverzhinsky A, Sarker M, Roy S, Malo C, Pascal
550 JM, Marko JF, D'Amours D. The Smc5/6 Core Complex Is a Structure-Specific DNA Binding
551 and Compacting Machine. Mol Cell. 2020;80(6):1025-38 e5. PMCID: PMC8224240
552 14. Jeppsson K, Pradhan B, Sutani T, Sakata T, Umeda Igarashi M, Berta DG, Kanno T,
553 Nakato R, Shirahige K, Kim E, Bjorkegren C. Loop-extruding Smc5/6 organizes transcription-
554 induced positive DNA supercoils. Mol Cell. 2024;84(5):867-82 e5.
555 15. Gutierrez-Escribano P, Hormeno S, Madariaga-Marcos J, Sole-Soler R, O'Reilly FJ,
556 Morris K, Aicart-Ramos C, Aramayo R, Montoya A, Kramer H, Rappsilber J, Torres-Rosell J,
557 Moreno-Herrero F, Aragon L. Purified Smc5/6 Complex Exhibits DNA Substrate Recognition
558 and Compaction. Mol Cell. 2020;80(6):1039-54 e6. PMCID: PMC7758880
559 16. Kim E, Barth R, Dekker C. Looping the Genome with SMC Complexes. Annu Rev
560 Biochem. 2023;92:15-41.
561 17. Uhlmann F. SMC complexes: from DNA to chromosomes. Nat Rev Mol Cell Biol. 2016.
562 18. Adamus M, Lelkes E, Potesil D, Ganji SR, Kolesar P, Zabrady K, Zdrahal Z, Palecek
563 JJ. Molecular Insights into the Architecture of the Human SMC5/6 Complex. J Mol Biol.
564 2020;432(13):3820-37.

565 19. Yu Y, Li S, Ser Z, Sanyal T, Choi K, Wan B, Kuang H, Sali A, Kentsis A, Patel DJ, Zhao
566 X. Integrative analysis reveals unique structural and functional features of the Smc5/6 complex.
567 Proc Natl Acad Sci U S A. 2021;118(19). PMCID: PMC8126833
568 20. Taschner M, Basquin J, Steigenberger B, Schafer IB, Soh YM, Basquin C, Lorentzen
569 E, Raschle M, Scheltema RA, Gruber S. Nse5/6 inhibits the Smc5/6 ATPase and modulates
570 DNA substrate binding. EMBO J. 2021;40(15):e107807. PMCID: PMC8327961
571 21. Li Q, Zhang J, Haluska C, Zhang X, Wang L, Liu G, Wang Z, Jin D, Cheng T, Wang H,
572 Tian Y, Wang X, Sun L, Zhao X, Chen Z, Wang L. Cryo-EM structures of Smc5/6 in multiple
573 states reveal its assembly and functional mechanisms. Nat Struct Mol Biol. 2024;31(10):1532-
574 42. PMCID: PMC11479838
575 22. Pradhan B, Kanno T, Umeda Igarashi M, Loke MS, Baaske MD, Wong JSK, Jeppsson
576 K, Bjorkegren C, Kim E. The Smc5/6 complex is a DNA loop-extruding motor. Nature.
577 2023;616(7958):843-8. PMCID: PMC10132971
578 23. Palecek JJ. SMC5/6: Multifunctional Player in Replication. Genes (Basel). 2018;10(1).
579 PMCID: PMC6356406
580 24. Ryu T, Spatola B, Delabaere L, Bowlin K, Hopp H, Kunitake R, Karpen GH, Chiolo I.
581 Heterochromatic breaks move to the nuclear periphery to continue recombinational repair. Nat
582 Cell Biol. 2015;17(11):1401-11. PMCID: PMC4628585
583 25. Palecek J, Vidot S, Feng M, Doherty AJ, Lehmann AR. The Smc5-Smc6 DNA repair
584 complex. bridging of the Smc5-Smc6 heads by the KLEISIN, Nse4, and non-Kleisin subunits. J
585 Biol Chem. 2006;281(48):36952-9.
586 26. Bustard DE, Ball LG, Cobb JA. Non-Smc element 5 (Nse5) of the Smc5/6 complex
587 interacts with SUMO pathway components. Biol Open. 2016;5(6):777-85. PMCID: PMC4920195

588 27. Oravcova M, Gadaleta MC, Nie M, Reubens MC, Limbo O, Russell P, Boddy MN. Brc1
589 Promotes the Focal Accumulation and SUMO Ligase Activity of Smc5-Smc6 during Replication
590 Stress. Mol Cell Biol. 2019;39(2). PMCID: PMC6321882
591 28. Pebernard S, Wohlschlegel J, McDonald WH, Yates JR, 3rd, Boddy MN. The Nse5-
592 Nse6 dimer mediates DNA repair roles of the Smc5-Smc6 complex. Mol Cell Biol.
593 2006;26(5):1617-30.
594 29. Wan B, Wu J, Meng X, Lei M, Zhao X. Molecular Basis for Control of Diverse Genome
595 Stability Factors by the Multi-BRCT Scaffold Rtt107. Mol Cell. 2019;75(2):238-51 e5. PMCID:
596 PMC6745058
597 30. Li S, Yu Y, Zheng J, Miller-Browne V, Ser Z, Kuang H, Patel DJ, Zhao X. Molecular
598 basis for Nse5-6 mediated regulation of Smc5/6 functions. Proc Natl Acad Sci U S A.
599 2023;120(45):e2310924120. PMCID: PMC10636319
600 31. Hallett ST, Schellenberger P, Zhou L, Beuron F, Morris E, Murray JM, Oliver AW.
601 Nse5/6 is a negative regulator of the ATPase activity of the Smc5/6 complex. Nucleic Acids
602 Res. 2021;49(8):4534-49. PMCID: PMC8096239
603 32. Etheridge TJ, Villahermosa D, Campillo-Funollet E, Herbert AD, Irmisch A, Watson AT,
604 Dang HQ, Osborne MA, Oliver AW, Carr AM, Murray JM. Live-cell single-molecule tracking
605 highlights requirements for stable Smc5/6 chromatin association in vivo. Elife. 2021;10. PMCID:
606 PMC8075580
607 33. Oravcova M, Nie M, Zilio N, Maeda S, Jami-Alahmadi Y, Lazzerini-Denchi E,
608 Wohlschlegel JA, Ulrich HD, Otomo T, Boddy MN. The Nse5/6-like SIMC1-SLF2 complex
609 localizes SMC5/6 to viral replication centers. Elife. 2022;11. PMCID: PMC9708086
610 34. Niu C, Livingston CM, Li L, Beran RK, Daffis S, Ramakrishnan D, Burdette D, Peiser L,
611 Salas E, Ramos H, Yu M, Cheng G, Strubin M, Delaney Iv WE, Fletcher SP. The Smc5/6
612 Complex Restricts HBV when Localized to ND10 without Inducing an Innate Immune Response

613 and Is Counteracted by the HBV X Protein Shortly after Infection. PLoS One.
614 2017;12(1):e0169648. PMCID: PMC5240991 does not alter our adherence to PLOS ONE
615 policies on sharing data and materials.
616 35. Ashkenazy H, Abadi S, Martz E, Chay O, Mayrose I, Pupko T, Ben-Tal N. ConSurf
617 2016: an improved methodology to estimate and visualize evolutionary conservation in
618 macromolecules. Nucleic Acids Res. 2016;44(W1):W344-50. PMCID: PMC4987940
619 36. Evans R, O'Neill M, Pritzel A, Antropova N, Senior A, Green T, Žídek A, Bates R,
620 Blackwell S, Yim J, Ronneberger O, Bodenstein S, Zielinski M, Bridgland A, Potapenko A,
621 Cowie A, Tunyasuvunakool K, Jain R, Clancy E, Kohli P, Jumper J, Hassabis D. Protein
622 complex prediction with AlphaFold-Multimer. bioRxiv. 2021:2021.10.04.463034.
623 37. Soboleski MR, Oaks J, Halford WP. Green fluorescent protein is a quantitative reporter
624 of gene expression in individual eukaryotic cells. FASEB J. 2005;19(3):440-2. PMCID:
625 PMC1242169
626 38. Cho T, Hoeg L, Setiaputra D, Durocher D. NFATC2IP is a mediator of SUMO-
627 dependent genome integrity. Genes Dev. 2024;38(5-6):233-52. PMCID: PMC11065178
628 39. Sun H, Hunter T. Poly-small ubiquitin-like modifier (PolySUMO)-binding proteins
629 identified through a string search. J Biol Chem. 2012;287(50):42071-83. PMCID: PMC3516753
630 40. Langston SP, Grossman S, England D, Afroze R, Bence N, Bowman D, Bump N, Chau
631 R, Chuang BC, Claiborne C, Cohen L, Connolly K, Duffey M, Durvasula N, Freeze S, Gallery M,
632 Galvin K, Gaulin J, Gershman R, Greenspan P, Grieves J, Guo J, Gulavita N, Hailu S, He X,
633 Hoar K, Hu Y, Hu Z, Ito M, Kim MS, Lane SW, Lok D, Lublinsky A, Mallender W, McIntyre C,
634 Minissale J, Mizutani H, Mizutani M, Molchinova N, Ono K, Patil A, Qian M, Riceberg J, Shindi
635 V, Sintchak MD, Song K, Soucy T, Wang Y, Xu H, Yang X, Zawadzka A, Zhang J, Pulukuri SM.
636 Discovery of TAK-981, a First-in-Class Inhibitor of SUMO-Activating Enzyme for the Treatment
637 of Cancer. J Med Chem. 2021;64(5):2501-20.

638 41. Boggio R, Colombo R, Hay RT, Draetta GF, Chiocca S. A mechanism for inhibiting the
639 SUMO pathway. Mol Cell. 2004;16(4):549-61.
640 42. Boulanger M, Chakraborty M, Tempe D, Piechaczyk M, Bossis G. SUMO and
641 Transcriptional Regulation: The Lessons of Large-Scale Proteomic, Modifomic and Genomic
642 Studies. Molecules. 2021;26(4). PMCID: PMC7915335
643 43. Yao Q, Peng B, Li C, Li X, Chen M, Zhou Z, Tang D, He J, Wu Y, Sun Y, Li W. SLF2
644 Interacts with the SMC5/6 Complex to Direct Hepatitis B Virus Episomal DNA to Promyelocytic
645 Leukemia Bodies for Transcriptional Repression. J Virol. 2023;97(7):e0032823. PMCID:
646 PMC10373549
647 44. Loe TK, Li JSZ, Zhang Y, Azeroglu B, Boddy MN, Denchi EL. Telomere length
648 heterogeneity in ALT cells is maintained by PML-dependent localization of the BTR complex to
649 telomeres. Genes Dev. 2020;34(9-10):650-62. PMCID: PMC7197349
650 45. Dupont L, Bloor S, Williamson JC, Cuesta SM, Shah R, Teixeira-Silva A, Naamati A,
651 Greenwood EJD, Sarafianos SG, Matheson NJ, Lehner PJ. The SMC5/6 complex compacts
652 and silences unintegrated HIV-1 DNA and is antagonized by Vpr. Cell Host Microbe.
653 2021;29(5):792-805 e6. PMCID: PMC8118623
654 46. Decorsiere A, Mueller H, van Breugel PC, Abdul F, Gerossier L, Beran RK, Livingston
655 CM, Niu C, Fletcher SP, Hantz O, Strubin M. Hepatitis B virus X protein identifies the Smc5/6
656 complex as a host restriction factor. Nature. 2016;531(7594):386-9.
657 47. Murphy CM, Xu Y, Li F, Nio K, Reszka-Blanco N, Li X, Wu Y, Yu Y, Xiong Y, Su L.
658 Hepatitis B Virus X Protein Promotes Degradation of SMC5/6 to Enhance HBV Replication. Cell
659 Rep. 2016;16(11):2846-54. PMCID: PMC5078993
660 48. Fine DA, Rozenblatt-Rosen O, Padi M, Korkhin A, James RL, Adelmant G, Yoon R,
661 Guo L, Berrios C, Zhang Y, Calderwood MA, Velmurgan S, Cheng J, Marto JA, Hill DE, Cusick
662 ME, Vidal M, Florens L, Washburn MP, Litovchick L, DeCaprio JA. Identification of FAM111A as

663 an SV40 host range restriction and adenovirus helper factor. PLoS Pathog.
664 2012;8(10):e1002949. PMCID: PMC3475652
665 49. Ngo AM, Puschnik AS. Genome-Scale Analysis of Cellular Restriction Factors That
666 Inhibit Transgene Expression from Adeno-Associated Virus Vectors. J Virol.
667 2023;97(4):e0194822. PMCID: PMC10134838
668 50. Irwan ID, Bogerd HP, Cullen BR. Epigenetic silencing by the SMC5/6 complex
669 mediates HIV-1 latency. Nat Microbiol. 2022;7(12):2101-13. PMCID: PMC9712108
670 51. Hofmann S, Plank V, Groitl P, Skvorc N, Hofmann K, Luther J, Ko C, Zimmerman P,
671 Bruss V, Stadler D, Carpentier A, Rezk S, Nassal M, Protzer U, Schreiner S. SUMO
672 Modification of Hepatitis B Virus Core Mediates Nuclear Entry, Promyelocytic Leukemia Nuclear
673 Body Association, and Efficient Formation of Covalently Closed Circular DNA. Microbiol Spectr.
674 2023;11(3):e0044623. PMCID: PMC10269885
675 52. Mearini G, Nielsen PE, Fackelmayer FO. Localization and dynamics of small circular
676 DNA in live mammalian nuclei. Nucleic Acids Res. 2004;32(8):2642-51. PMCID: PMC419472
677 53. Zhao R, Xu M, Yu X, Wondisford AR, Lackner RM, Salsman J, Dellaire G, Chenoweth
678 DM, O'Sullivan RJ, Zhao X, Zhang H. SUMO promotes DNA repair protein collaboration to
679 support alternative telomere lengthening in the absence of PML. Genes Dev. 2024;38(13-
680 14):614-30. PMCID: PMC11368244
681 54. Sullivan CS, Pipas JM. T antigens of simian virus 40: molecular chaperones for viral
682 replication and tumorigenesis. Microbiol Mol Biol Rev. 2002;66(2):179-202. PMCID:
683 PMC120785
684 55. Gilinger G, Alwine JC. Transcriptional activation by simian virus 40 large T antigen:
685 requirements for simple promoter structures containing either TATA or initiator elements with
686 variable upstream factor binding sites. J Virol. 1993;67(11):6682-8. PMCID: PMC238107

687 56. Qadri I, Conaway JW, Conaway RC, Schaack J, Siddiqui A. Hepatitis B virus
688 transactivator protein, HBx, associates with the components of TFIIH and stimulates the DNA
689 helicase activity of TFIIH. Proc Natl Acad Sci U S A. 1996;93(20):10578-83. PMCID: PMC38195
690 57. Aufiero B, Schneider RJ. The hepatitis B virus X-gene product trans-activates both
691 RNA polymerase II and III promoters. EMBO J. 1990;9(2):497-504. PMCID: PMC551692
692 58. Felzien LK, Woffendin C, Hottiger MO, Subbramanian RA, Cohen EA, Nabel GJ. HIV
693 transcriptional activation by the accessory protein, VPR, is mediated by the p300 co-activator.
694 Proc Natl Acad Sci U S A. 1998;95(9):5281-6. PMCID: PMC20252
695 59. Ahuja D, Saenz-Robles MT, Pipas JM. SV40 large T antigen targets multiple cellular
696 pathways to elicit cellular transformation. Oncogene. 2005;24(52):7729-45.
697 60. Googins MR, An P, Gauthier CH, Pipas JM. Polyomavirus large T antigens: Unraveling
698 a complex interactome. Tumour Virus Res. 2024;19:200306. PMCID: PMC11720896
699 61. Tampere M, Mortusewicz O. DNA Damage Induction by Laser Microirradiation. Bio-
700 protocol 2016;6(23):e2039.
701
702
703
704

705 **Acknowledgements**

706 This work was supported by NIH grants R35 GM136273 to M.N.B. and GM092740 to T.O.

707

708 **Author information**

709 Affiliations

710 **Department of Molecular and Cellular Biology, The Scripps Research Institute, La**

711 **Jolla, CA 92037, USA.**

712 Martina Oravcová, Minghua Nie & Michael N. Boddy

713

714 **San Diego Biomedical Research Institute, San Diego, CA 92121, USA.**

715 Takanori Otomo

716

717 Contributions

718 Conceptualization, M.N.B., T.O. Design of Methodology, M.O., M.N., M.N.B., T.O. Writing

719 – Original Draft, M.N.B., M.N., T.O. Writing – Review & Editing, M.O., M.N., T.O., M.N.B.

720 Formal analysis/Investigation, M.O., M.N., M.N.B., T.O. Validation, M.O., M.N. Resources,

721 M.O., M.N. Visualization, M.O., M.N., T.O., M.N.B. Funding acquisition, M.N.B., T.O.

722 Supervision, M.N.B., T.O. Project administration, M.N.B.

723

724 Corresponding authors:

725 Correspondence to Michael N. Boddy and Takanori Otomo.

726

Ethics declarations

Competing interests

The authors declare no competing interests.

731 **Supplementary figures:**

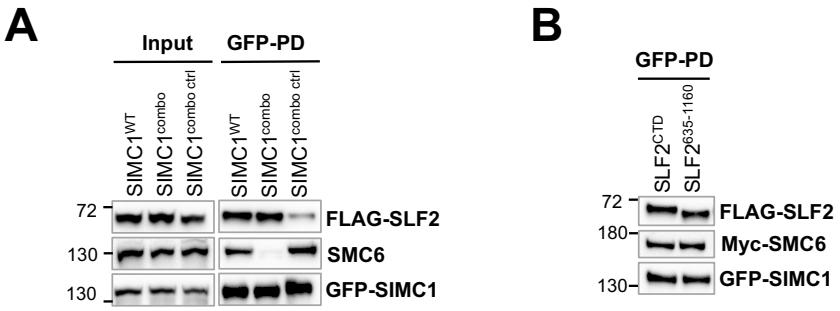

732
733
734 **Figure 1 - figure supplement 1.**
735 **(A)** Western blot of GFP-trap immunoprecipitation from HEK293 cells transiently
736 transfected respectively with GFP-SIMC1, GFP-SIMC1 combo mutant or GFP-SIMC1
737 combo control mutant in combination with FLAG-SLF2^{CTD} and Myc-SMC6. Signals were
738 detected using FLAG, SMC6 and GFP antibodies. **(B)** Western blot of GFP-trap
739 immunoprecipitation from HEK293 cells transiently transfected with either FLAG-SLF2^{CTD}
740 or FLAG-SLF2$^{635-1160}$ co-transfected with GFP-SIMC1 and Myc-SMC6. Signals were
741 visualized using FLAG, Myc and GFP antibodies.
742

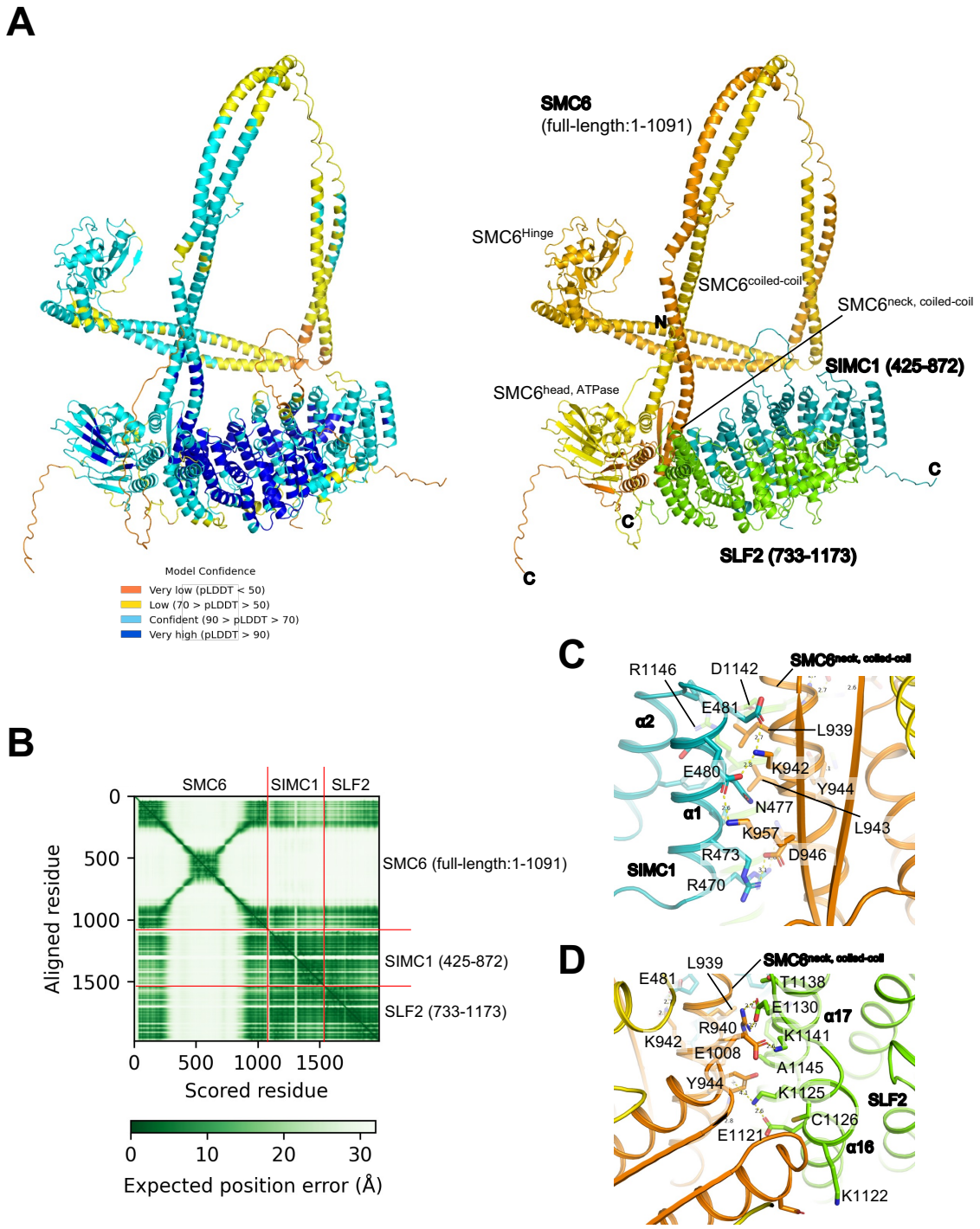

Figure 2 - figure supplement 1

(A) The AlphaFold-Multimer model of the SIMC1^{Nse5} (425-872)-SLF2^{Nse6} (733-1173)-SMC6 (1-1091) complex. The entire model is shown, colored according to pLDDT values (left) or in the same manner as in **Figure 2A**. **(B)** The Predicted Aligned Error (PAE) plot of the AlphaFold-Multimer prediction. **(C, D)** Close-up views of the SMC6 neck-SIMC1 (C) and SMC6 neck-SLF2 (D) interfaces.

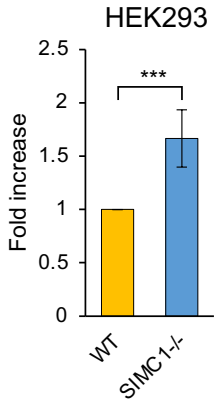

751
752 **Figure 3 - figure supplement 1**
753 HEK293 WT or SIMC1$^{-/-}$ cells were transiently transfected with GFP reporter and GFP
754 intensity was assessed 72 hours later by FACS. Data are the average ± s.d. from n=6
755 independent experiments, two-tailed unpaired t-test; (***) $p<0.0005$).

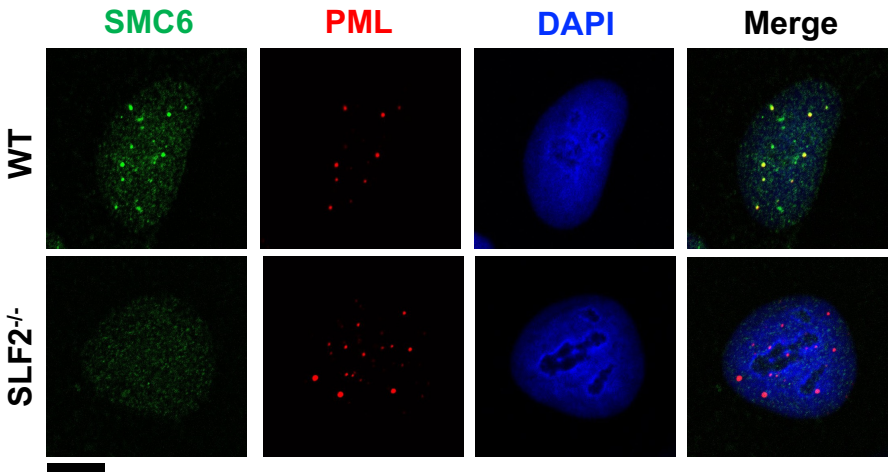

Figure 5 - figure supplement 1

Representative immunofluorescence images of U2OS WT or SLF2$^{-/-}$ cells fixed and stained with SMC6 (green) and PML (red) antibodies along with DAPI (blue). Scale bar 10 μm.

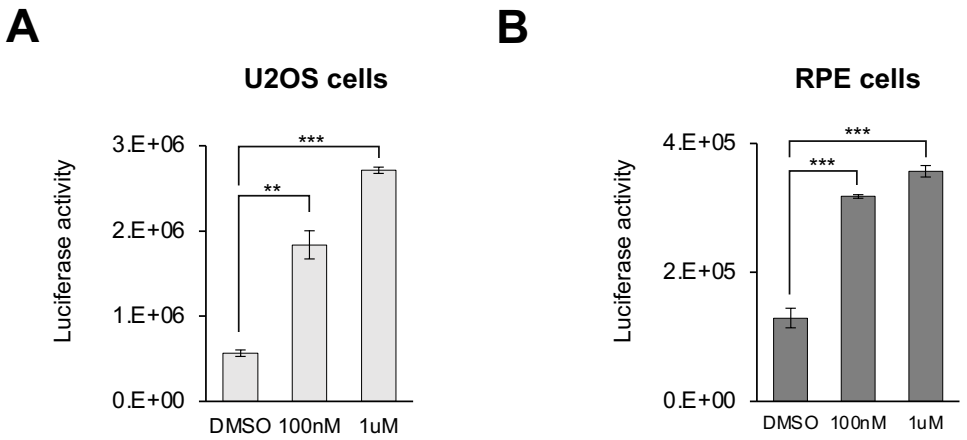

Figure 5 - figure supplement 2

Arbitrary luminescence units of U2OS (**A**) or RPE (**B**) cells expressing transfected pLuc reporter. Cells were treated with TAK-981 or DMSO at the time of transfection. Means and error bars (s.d.) were derived from a minimum of n=3 independent transfections representing biological replicates. Two-tailed unpaired t-test was performed ((∗∗) $p<0.005$; (∗∗∗) $p<0.0005$).

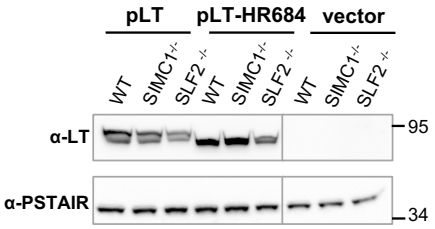

Figure 5 - figure supplement 3

Immunoblot from U2OS WT, SIMC1$^{-/-}$ or SLF2$^{-/-}$ cells stably expressing large T antigen (LT), LT-HR684 variant or have an empty vector integrated, respectively. PSTAIR serves as a loading control.

773

774 **List of Supplementary files**

775 Figure 1—figure supplement 1. A, B

776 Figure 2—figure supplement 1. A-D

777 Figure 3—figure supplement 1

778 Figure 5—figure supplement 1.

779 Figure 5—figure supplement 2. A, B.

780 Figure 5—figure supplement 3.

781

782 **List of source data**

783 Figure 1 – source data 1. Full and unedited blots corresponding to panel C.

784 Figure 2 – source data 1. Full and unedited blots corresponding to panel C.

785 Figure 3 – source data 1. GFP transcripts qPCR corresponding to panel A.

786 Figure 3 – source data 2. GFP FACS corresponding to panel B.

787 Figure 4 – source data 1. GFP FACS corresponding to panel B.

788 Figure 5 – source data 1. GFP FACS corresponding to panel A.

789 Figure 5 – source data 2. GFP FACS corresponding to panel B.

790 Figure 5 – source data 3. Full and unedited blots corresponding to panel C.

791 Figure 5 – source data 4. GFP FACS corresponding to panel D.

792 Figure 1 – figure supplement 1 – source data 1. Full and unedited blots corresponding

793 to panel A.

794 Figure 1 – figure supplement 1 – source data 2. Full and unedited blots corresponding

795 to panel B.

796 Figure 3 – figure supplement 1 - source data 1. GFP FACS.

797 Figure 5 – figure supplement 2 - source data 1. Luciferase measurement corresponding

798 to panel A.

799 Figure 5 – figure supplement 2 - source data 2. Luciferase measurement corresponding

800 to panel B.

801 Figure 5 – figure supplement 3 - source data 1. Full and unedited blots.

802
803